ALICE: Physics with electrons

R. SCHICKER, FOR THE ALICE COLLABORATION

Physikalisches Institut, University of Heidelberg, 69120 Heidelberg, Germany

Received 23 December 2004;
final version 23 December 2004

The ALICE potential for measurements of dielectron decays of quarkonia J/Ψ and of the Υ-family is discussed. The electron trigger capability of the ALICE transition radiation detector (TRD) is reviewed, and the anticipated pion rejection power is given. Furthermore, the invariant mass resolution achieved for quarkonia states is given and the signal to background ratio is presented.

Key words: Quarkonia, dielectron decays

1 Introduction

Heavy quarks and quarkonia $J/\Psi, \Psi', \Upsilon, \Upsilon', \Upsilon''$ produced in heavy ion collisions are of great interest as probes of the nuclear collision dynamics. In particular, the dissociation of quarkonia states is one of the most important observable for the existence of a deconfined state. The suppression of quarkonia states is due to the shielding of potential by Debye screening [1]. A quantitative characterization of dissociation temperature depends, however, on the structure of heavy quark potential at high temperature. Information on this potential can be extracted by an analysis of heavy quark free energies on the lattice [2]. While some authors claim an abrupt J/Ψ dissociation at $T = 1.9\,T_c$, others conclude a rather gradual J/Ψ dissociation with complete disappearance only at $T = 3.0\,T_c$ [3, 4].

In order to be reliable probes in nucleus-nucleus collisions, the cross sections for heavy quark and quarkonia production need to be known in proton-proton collisions. Theoretical predictions for the $c\overline{c}$-pair production cross section in pp collisions at 14 TeV are in the range 7-17 mb depending on the values used for the charm mass and for the factorization and renormalization scale [5]. The K-factors quantifying next to leading order corrections are between 1.7 and 2.1 for the different parameterizations and hence make rate estimates uncertain. The ratios of cross sections at 14 TeV to 5.5 TeV agree, on the other hand, within the parameter sets to a few percent. In the case of bottom pairs in pp-collisions at 14 TeV, the different parameter sets result in $b\overline{b}$ production cross sections between 0.2 and 0.7 mb. The K-factors range from 1.4 to 3.2 and again make rate estimates uncertain.

Production rates in AA collisions are affected by modifications of parton distribution functions in the nucleus. The nuclear gluon distribution is significantly affected by parton dynamics in the small x-region and is expected to be substantially reduced as compared to the distribution in the nucleon. The relevant x-value for charm production in the ALICE central barrel is x$\sim 10^{-4}$, and is about 2 orders of magnitude lower than at RHIC. Although the nuclear gluon distribution is not well known, it is accessible through a comparison of pA collisions relative to pp.

The quarkonia rates can be modified by nuclear absorption and by secondary scatterings with comovers. These reactions can break up the quarkonia states and hence reduce the expected rates. The large number of $Q\overline{Q}$ pairs produced at LHC energies could, however, be an abundant source of final state quarkonia by coalescence. This mechanism could result in an enhanced quarkonia production at LHC energies in contrast to the suppression discussed above [6, 7].

The complexity of heavy quark physics at LHC energies calls for comprehensive measurements of heavy quark and quarkonia production in pp, pA and AA collisions. Such a program is a continuation and extension of ongoing efforts at different laboratories. At the SPS fixed target program, experiments NA38/NA50/NA60 measure J/Ψ production since 1986 [8]. At the relativistic heavy ion collider RHIC, experimental efforts have been started by the PHENIX experiment[9].

2 Transition Radiation Detector

The ALICE Transition Radiation Detector (TRD) provides electron identification in the ALICE central barrel for transverse momenta $P_T \geq 1$ GeV/c [10]. The TRD hence complements the electron identification for momenta $P_T \leq 1$ GeV/c achieved by energy loss measurements in the Time Projection Chamber (TPC).

Measurement of J/Ψ and its P_T-dependence requires a pion rejection factor better than 100 for $P_T \geq 3$ GeV/c. The dielectron continuum between J/Ψ and Υ requires the same rejection power. The position and momentum resolution of the TRD must be good enough to allow for track matching between TPC and TRD.

The coverage in pseudorapidity of the TRD is matched to the pseudorapidity acceptance of the ALICE central barrel $|\eta| \leq 0.9$ [11]. The TRD detector is located at a radial distance r (2.9 m $\leq$ r $\leq$ 3.7 m) from the beam axis, hence the TRD system covers a maximum of 7 m in z-direction. The 18-fold azimuthal and five-fold longitudinal segmentation results in maximum chamber dimensions of 120 x 159 cm^2. The necessary pion rejection factor as defined above can be achieved by six modules stacked in radial direction. The TRD system therefore consists of a total of 540 detector modules.

3 Detector module

The detector modules consist of radiator material producing the TR photons and a readout chamber. As the average energy of emitted TR photon is approximately proportional to the Lorentz factor γ of the particle (for γ around a few thousand), electrons and pions can be well separated in the momentum range of a few GeV/c by their different TR photon emission characteristics.

A schematic view of a detector module is shown in Fig.1 on the left. The TR photons produced by electrons in the radiator get absorbed in the 30 mm drift volume which is filled with a Xe-CO_2 mixture (85-15). The distance between cathode wires and read out pads as indicated by the amplification region is 7 mm. The signal on the cathode is typically spread over 2-3 pads of dimensions 90x10 mm^2.

Eighteen adjacent pads are combined and connected to a flat ribbon cable. The pad signals are processed in a custom built preamplifier-shaper circuit and digitized by a 10 MHz ADC. The drift time of about 2.0 μs hence results in about 20 time bins.

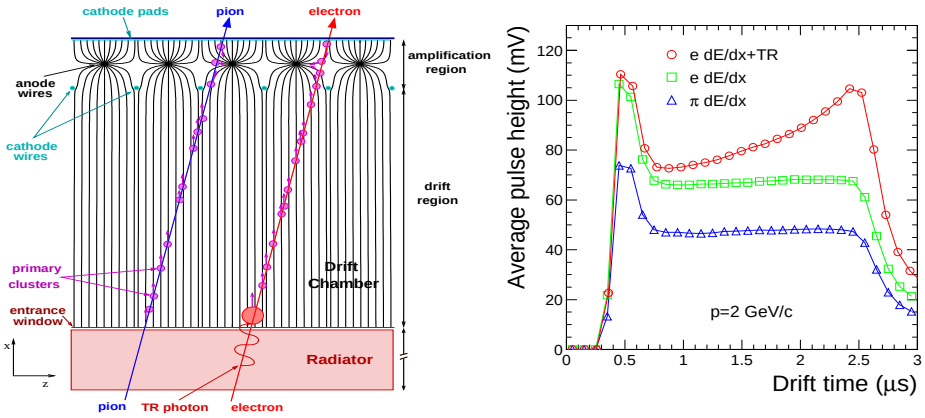

Fig. 1. Detector module is shown on the left with a pion and an electron trajectory. A pulse height spectrum is shown on the right

.

The right hand side of Fig.1 shows average pulse heights measured in the TRD chamber for both pions and electrons of momenta 2 GeV/c as a function of drift time. The peak at early drift times is generated by the charge deposited in the amplification region. This charge drifts to the anode from both sides and hence generates a large signal. The pion spectrum as shown by the triangle symbols is rather flat at larger drift times and represents the pion energy loss within the drift space volume. Electrons, on the other hand, show the additional component of the TR photon contribution as indicated by the open circles. This contribution is peaked at late times since TR photons are absorbed in the drift volume mainly close to the radiator with correspondingly long drift times to the anode.

4 Electron trigger

An online trigger is required to tag events which contain high P_T electron tracks. The 20 time samples of the ADC are fed into a digital chip for tail cancellation of the signal. The data are subsequently processed by the local tracking unit (LTU). This LTU calculates the hit position in each time bin by using the measured pad response function. Local tracklets are built by fitting straight lines to the hits in the different time bins. An electron likelihood factor based on integrated charge is associated to each tracklet. The information from the different LTU units is subsequently fed into the global tracking unit (GTU). This GTU unit associates tracklets to tracks and fits the track parameters. The track electron likelihood function is derived from the tracklet likelihood information. The performance of this online trigger is extensively studied in simulations [12].

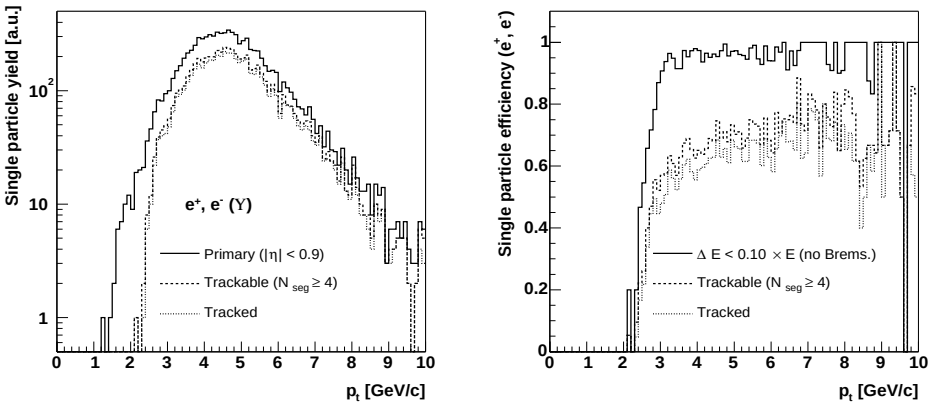

Fig. 2. Particle yield for Υ decays on the left. Efficiencies are shown on the right.

The solid line on the left in Fig.2 shows the yield of primary tracks in the central barrel for a sample of Υ decays. The dashed line represents the trackable yield, i.e. the tracks for which tracklets have been reconstructed in at least four layers. This track reconstruction includes a vertex constraint and a programmable transverse momentum cut with a minimum value of 1 GeV/c. The loss of yield is due to geometrical coverage in azimuthal and longitudinal direction within $|\eta| \leq 0.9$ as well as to kinks in electron tracks due to bremsstrahlung. The single particle efficiency is shown in Fig.2 on the right. The dashed line represents the ratio of trackable to primary tracks. The ratio of tracked to primary tracks is shown by the dotted histogram. The tracked yield is smaller than the trackable due to the cuts defined in the GTU for handling the combinatorial possibilities of associating tracklets to tracks. The solid line represents the tracking efficiency for a sample of tracks which have lost less than 10% of their vertex energy when exiting the TRD.

5 Pion rejection

The pion rejection factors shown in Fig.3 on the left by the open circles represent the measured performance of a stack of 4 TRD chambers. The pion rejection for 5 and 6 chambers as indicated by the triangles is extrapolated by an analysis in which the electron identification is based on total charge and is kept at 90%. The performance of six layers fulfills the requirements of pion rejection factor larger than 100 for physics measurements in the quarkonia sector.

The pion efficiency of a stack of 6 chambers is shown in Fig.3 on the right as a function of momentum. Here, the particle identification is based on a two-dimensional likelihood function. In this approach, a second, independent likelihood factor is calculated based on the time information of the maximum deposited charge. The pion efficiencies shown are achieved at an electron efficiency of 90%.

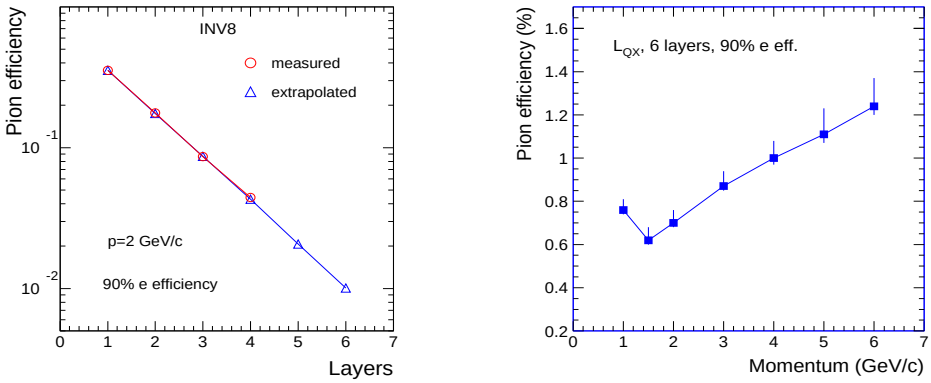

Fig. 3. Pion efficiency as function of number of layers is shown on the left. On the right, pion efficiency as function of momentum.

6 Quarkonia signal $J/\Psi, \Upsilon$

The position information derived from one TRD chamber is about 400 μm in phi-direction. The information from the total stack of six chambers contributes to the performance of the combined tracking ITS-TPC-TRD predominantly at high transverse momenta due to the large leverarm of the TRD. At transverse momenta relevant for quarkonia decays, the resolution dP_T/P_T at $P_T = 1$ GeV/c and 5 GeV/c has been shown to be 1% and 1.8 %, respectively [13].

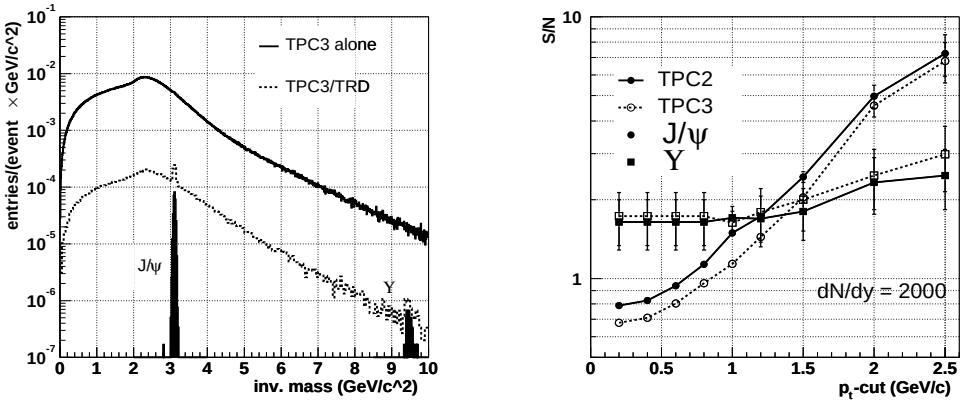

Fig. 4. Dielectron mass spectrum on the left. The signal to noise ratio S/N on the right.

Fig.4 on the left shows a simulated invariant dielectron mass spectrum for a sample of Pb-Pb events with a 10% centrality cut[14]. In these simulations, the HIJING model generates the charged pions representing a rapidity density dN/dy = 2000.

The quarkonia signals in the dielectron decay channel amount to 0.03 J/Ψ and 4×10^{-4} Υ per event. The mass spectrum as indicated by the solid line is derived by TPC information only. This sample contains pions which are misidentified based on the dE/dx resolution of the TPC. The dashed line includes the electron identification of the TRD which reduces the combinatorial background by more than an order of magnitude. In particular, the mass region of the Υ-family would not be accessible based on TPC information only.

The ratio signal to noise S/N as function of a single track P_t-cut is shown in Fig.4 on the right. The background from semileptonic decays of D and B mesons as well as misidentified pions are concentrated at lower transverse momentum P_t. The signal to background ratio can therefore be optimized by a judicious choice of such a cut. Here, the two curves TPC2 and TPC3 represent two different pion efficiencies based on different TPC scenarios.

The anticipated mass resolution has been evaluated for combined TRD-TPC tracking. The calculated resolution for J/Ψ and Υ is about $\sigma^M_{J/\Psi} \sim 27$ MeV/c^2 and $\sigma^M_{\Upsilon} \sim 75$ MeV/c^2, respectively. These values indicate the Υ-family to be well separated since the Υ and $\Upsilon^{'}$ mass differ by about 7 standard deviations, whereas the separation between $\Upsilon^{'}$ and $\Upsilon^{''}$ mass is about 4 standard deviations.

7 Acknowledgements

This work was supported in part by the German BMBF under project 06HD160I.

References

[1] T.Matsui and H.Satz, Phys.Lett. B **178** (1986) 416

[2] F.Karsch, J.Phys.**G30** (2004) 887

[3] M.Asakawa and T.Hatsuda, Phys.Rev.Lett. **92** (2004) 012001

[4] S.Datta, F.Karsch, P.Petreczky and I.Wetzorke, Phys.Rev. **D69**, (2004) 094507

[5] Heavy flavour physics, Hard probes in HI collisions at the LHC, hep-ph/0311048

[6] P.Braun-Munzinger and J.Stachel, Phys.Lett.B **490** (2000) 196

[7] R.Thews and J.Rafelski, Nucl. Phys. A **698** (2002) 575

[8] R.Arnaldi, Hard Probes Conference 2004, Nov 2004, Ericeira

[9] R.G.deCassagnac, J.Phys.**G30** (2004) 1341

[10] ALICE, Technical design report of Transition Radiation Detector, CERN/LHCC 2001-021, Oct 2001

[11] Ch.Fabjan, ALICE at LHC, LHCPH2004, July 2004, Vienna

[12] B. Vulpescu, ALICE TRD trigger algorithms and performance for Upsilon detection, HERA and the LHC workshop, March 2004, CERN

[13] K. Safarik, Physics program of ALICE, Europhys. Conf. NPDC18, Aug 2004, Prague

[14] T. Mahmoud, Development of readout chamber of the ALICE Transition Detector and Evaluation of its Physics Performance, Doctoral thesis, Heidelberg 2004